A&A manuscript no. (will be inserted by hand later)	ASTRONOMY
Your thesaurus codes are: 20(04.19.1; 09.19.1; 10.07.1; 13.18.3)	ASTROPHYSICS

# A 1.4 GHz radio continuum and polarization survey at medium Galactic latitudes:

# II. First section

B. Uyanıker, E. Fürst, W. Reich, P. Reich, and R. Wielebinski

Max-Planck-Institut für Radioastronomie, Postfach 2024, 53010 Bonn, Germany

Received 30 September 1998 / Accepted 8 April 1999

**Abstract.** We present the first section of a radio continuum and polarization survey at medium Galactic latitudes carried out with the Effelsberg 100-m telescope at 1.4 GHz. Four large fields have been observed, which all together cover an area of about  $1100 \square$ . The rms-sensitivity is about 15 mK T<sub>B</sub> (about 7 mJy/beam area) in total intensity and is limited by confusion. A sensitivity of 8 mK T<sub>B</sub> is obtained in linear polarization. The angular resolution of the observations is 9.35. The maps in total intensity and linear polarization have been absolutely calibrated by low resolution data where available. Significant linear polarization is seen in all the maps. In general, the intensity fluctuations measured in linear polarization are not correlated with total intensity structures. Areas of high polarization of some degrees extent are seen, again with no apparent corresponding total intensity feature. Modulation of polarized background emission by spatially varying Faraday rotation seems the most likely explanation. Quite unexpected is the detection of filamentary and ring-like depolarization structures in the direction of the anticentre region, whose extents are up to about  $3^{\circ}$ .

**Key words:** Surveys – Galaxy: structure – Radio continuum – linear polarization – Interstellar magnetic fields

# 1. Introduction

Our knowledge of the Galactic magnetic field at present is primarily based on studies of the distribution of rotation measures of pulsars or extragalactic sources and optical observations of polarized star light (e.g. Wielebinski 1992, Beck et al. 1996). In addition, early radio polarization surveys at low frequencies have revealed substantial linear polarization from the diffuse Galactic emission, implying the general presence of ordered magnetic fields. However, these early results were limited by low angular resolution and sensitivity. Also Faraday rotation effects are significant at low frequencies.

A polarimetric survey of the northern Galactic plane has been made by Junkes et al. (1987a) and Duncan et al. (1998) at 2695 MHz with the Effelsberg 100-m telescope. Complementary observations have been made with the Parkes 64-m telescope of a strip of the southern Galactic plane at 2400 MHz by Duncan et al. (1997). These observations revealed polarized emission of the diffuse Galactic radiation. At least some of these emission features are believed to originate at distances up to a few kpc (Junkes et al. 1987b). The medium and high latitudes of the Galaxy have not been studied in a systematic way. Surprisingly, observations at 327 MHz by Wieringa et al. (1993) carried out with the Westerbork radio telescope revealed filamentary polarized structures on a degree scale. These high Galactic latitude features are not detected at higher frequencies and have no counterpart in total intensity. Recently, Gray et al. (1998) detected at 1.4 GHz an interstellar Faraday rotation feature about 2° in size located in front of the prominent HII region W5. These results call for a systematic observational approach.

There exist already a Galactic plane survey at 1.4 GHz (Reich et al. 1990a, 1997) carried out with the Effelsberg telescope, which covers absolute Galactic latitudes of 4°. However, this survey does not include measurements of linearly polarized intensities. Meanwhile, a new sensitive receiver is available and we have started a sensitive survey of the radio continuum and polarized emission at medium Galactic latitudes with the Effelsberg telescope.

In a first paper (Uyanıker et al. 1998, Paper I) we have described the methods of observation and data reduction. In addition, we explained the procedure of absolute calibration of both the total intensity data from the Stockert 1.4 GHz survey (Reich 1982, Reich & Reich 1986) and the linear polarization data by 1.4 GHz observations made with the Dwingeloo 25-m telescope (Brouw & Spoelstra 1976). The medium latitude Effelsberg survey aims to observe regions at Galactic latitudes ( $|b| \leq 20^{\circ}$ ) accessible to the telescope.

The areas presented in this paper cover four fields. From the first Galactic quadrant an area of  $10^{\circ} \times 16^{\circ}$ 

centered on  $\ell=50^\circ$ ,  $b=12^\circ$  has been observed. Here the Dwingeloo polarization data could not be used because of a low S/N-ratio in general. The Cygnus-X area is the second region. This field includes the Cygnus superbubble, which is particularly bright in X-ray emission. The third area is the highly polarized region just above the Galactic plane between  $140^\circ \le \ell \le 153^\circ$ . In the anticentre a field of  $20^\circ \times 11^\circ$ 2 centered on  $\ell=200^\circ$ ,  $b=9^\circ$ 4 was surveyed. For this region no Dwingeloo polarization data are available for an absolute calibration.

In Sect. 2 we summarize some technical aspects. In Sect. 3 we show that the total intensity data are limited by confusion and we compare counts of compact sources with those based on the recent 1.4 GHz NVSS survey. The total intensity and polarimetric observations are displayed in Sect. 4, where in addition some comments on the individual fields are given.

# 2. The Survey: first section

The observations have been made with the two channel HEMT 1.3-1.7 GHz receiver installed in the primaryfocus of the Effelsberg 100-m telescope. The method of observation is to scan each field along Galactic latitude and longitude. Both coverages are combined as described in Paper I. The half-power-beam-width at 1.4 GHz is  $9.35 \pm 0.04$ . The conversion factor from main beam brightness temperature T<sub>B</sub> to flux density/beam area is  $2.12 \pm 0.02$ . Details of the data reduction are given in Paper I, where we also describe the method to reduce the instrumental polarization to a level of about 1%. The total intensity maps have been calibrated to an absolute scale using the Stockert 1.4 GHz survey and the polarization data by Dwingeloo 1.4 GHz data. Unfortunately, the Dwingeloo survey is incomplete. For some areas the data are severely undersampled or a have a low S/N-ratio.

# 3. Sensitivity, compact sources and confusion limit

All total intensity survey maps show a large number of compact sources, which are mainly of extragalactic origin. We have selected several small flat and empty fields from the survey maps and subtracted sources when necessary. The measured rms-noise is typically about 15 mK  $T_{\rm B}.$  No problem with confusing sources exists for polarized intensities, where a typical rms-noise value of 8 mK  $T_{\rm B}$  has been found.

The measured rms-noise in total intensity is about a factor of three larger than that calculated from the system temperature of about 30 K. Source confusion is believed to be the limiting factor in sensitivity. Condon et al. (1989) have studied the effect of source confusion for the former 300-ft Green-Bank telescope, which is described by  $\Delta S_c = 50 \, \nu^{-2.7}$ , where  $\nu$  is in GHz and  $\Delta S_c$  is the rms of intensity fluctuations in units of mJy/300-ft beam

Fig. 1. Source counts from an area in the Galactic anticentre as described in Sect. 3.

area. When calculating the expected confusion for the 100-m telescope from that approach we get about 16 mJy or 35 mK  $T_{\rm B}$  at 1.4 GHz, which is significantly larger than the measured rms-noise of 15 mK  $T_{\rm B}$  in the maps. We conclude that source confusion is significantly smaller than previously thought, but it is limiting the sensitivity for total intensities of the survey.

We have performed source counts from the survey maps based on a fitted two-dimensional Gaussian to each source. These counts have been compared with counts based on the recent 1.4 GHz VLA-survey (NVSS) by Condon et al. (1998), which is more sensitive to compact sources than our survey and suffers less from confusion due to its smaller beam size. We convolved a VLA map covering about  $71.5 \square$  to the angular resolution of the Effelsberg map and applied the same source fitting procedure to both maps. In Fig. 1 we show cumulative source counts for a region in the Galactic anticentre. We have also fitted the VLA data at their original angular resolution and found 910 sources in total. The corresponding cumulative source counts are also shown in Fig. 1 with a slope of about -1.4. This is close to the expected value of -1.5 for a uniform source density in the local universe. Source evolution and different source populations cause deviations from the -1.5 slope for sources weaker than about 100 mJy (see Condon et al. 1998 for details). Below about 40 mJy the fraction of sources which can not be fitted individually increases with decreasing flux density. For the Effelsberg data as well as for the convolved VLA data we obtain the same result over the entire flux density range. However, the deviation from the straight line starts already near 100 mJy. This effect is caused by the much larger confusion in the low resolution data: The total number of sources stronger than 10 mJy found in the original VLA data results in a mean source separation of about 22 VLA beam areas, but just about 1.8 beam areas of the 100-m telescope. Therefore, flux densities lower than about 100 mJy source counts are more complete, when using the original VLA data. With decreasing flux density an increasing fraction of sources cannot be fitted individually due to increasing confusion effects.

#### 4. Results

We present the results of our observations in the form of contour and grey-scale maps. The maps are also available in FITS-format via Internet (http://www.mpifr-bonn.mpg.de/survey.html).

When adding the absolutely calibrated large-scale emission to the Effelsberg data in both total and polarized intensity, much of the small-scale details are hidden in large-scale intensity gradients. We therefore separated the small and large-scale structures from each other using the "background filtering method" (Sofue & Reich 1979), which is based on an unsharp masking operation. This procedure has been applied to all absolutely calibrated total intensity maps. We separated emission on scales larger than about 3° from compact sources and emission on smaller scales. The sum of both components is exactly the original intensity. This procedure and presentation of data has been already applied for the Effelsberg Galactic plane surveys at 1.4 GHz (Reich et al. 1990a, 1997) and 2.695 MHz (Reich et al. 1990b, Fürst et al. 1990).

# 4.1. The area centered on $\ell = 50^{\circ}, b = 12^{\circ}$

Fig. 2 shows the small-scale total intensity emission with superimposed polarization vectors in E-field direction. Fig. 3 shows the corresponding large-scale emission in total intensity and polarized intensities are shown in Fig. 4.

This field of  $160 \,\Box$  is located between the North Polar Spur to the west and the Cygnus-X region to the east, which both contain strong emission from local sources. The observed field seems less affected by local features and thus more representative for the medium latitude emission from the inner part of the Galaxy. The total intensity decreases smoothly with latitude (Fig. 3). Significant intensity variations in the small-scale total intensity up to  $20^{\circ}$  latitude are visible in Fig. 2. The polarized intensities (Fig. 4) vary on small scales, but become more uniform for latitudes above  $16^{\circ}$ . A chain of high-velocity H I-clouds extending from  $\ell = 70^{\circ}$ ,  $b = 25^{\circ}$  towards the Galactic plane terminates close to  $\ell = 52^{\circ}$ ,  $b = 10^{\circ}$ , where enhanced synchrotron emission is visible as discussed by Uyanıker (1997).

#### 4.2. The Cygnus superbubble

Fig. 5 shows the small-scale emission of the southern and northern part of the Cygnus-X area in the same presentation as for Fig. 2. In Fig. 6 the corresponding large-scale total intensities are given and polarized intensities are shown in Fig. 7.

The particular interest in this region arises from the large X-ray halo surrounding the Cygnus-X area, called the Cygnus superbubble (Cash et al. 1980). The Cygnus-X area is a quite strong and rather complex region in the radio range, since the line of sight is along the local spiral arm. No sensitive radio surveys of the area of the Cygnus superbubble exist so far and we will discuss the relation of the X-ray emission revealed by ROSAT during its all-sky survey with the 1.4 GHz radio emission in a forthcoming paper. Highly varying and strong polarized intensity is seen in some areas, where the total intensity images show rather smooth emission. In particular the regions centered around  $\ell = 75^{\circ}$ ,  $b = -12^{\circ}$  south of the Cygnus loop ( $\ell =$  $74^{\circ}$ ,  $b = -8^{\circ}$ ), the large emission feature almost filling the field of view and crossing the map diagonally and the structure at  $\ell = 94^{\circ}$ ,  $b = -5^{\circ}$  about  $3^{\circ}$  in size should be mentioned.

Some well-known polarized objects are visible. These are three supernova remnants: the Cygnus loop, HB21 ( $\ell=89^\circ$ ,  $b=5^\circ$ ) and W63 ( $\ell=82^\circ$ ,  $b=5^\circ$ 5). At  $\ell=76^\circ$ ,  $b=6^\circ$  the exceptionally strong emission from the radio galaxy Cygnus A shows up. Telescope sidelobes from the four support legs of the subreflector show up to about  $4^\circ$  distance from the source in total intensity (Fig. 5) and slightly less in polarized intensity (Fig. 7).

# 4.3. The highly polarized region near $\ell = 140^{\circ}$

Fig. 8 shows the area from  $140^{\circ} \leq \ell \leq 153^{\circ}$  similar to Fig. 2, but polarization vectors represent the small-scale emission component. To separate the small-scale polarization structures, the strong sources are clipped in the absolutely calibrated U and Q maps and these maps are convolved to  $3^{\circ}$ . The convolved maps are subtracted from the original U and Q maps and the polarized intensity maps are prepared. Fig. 9 is the corresponding large-scale emission in total intensity with superimposed polarization vectors from the large-scale component. Polarized intensities are shown in Fig. 10 (small-scale emission) and Fig. 11 (large-scale emission), respectively.

Early polarization surveys as reviewed by Salter & Brown (1988) already revealed an outstanding polarized region with more than  $20^{\circ}$  in extent centered roughly at  $\ell=140^{\circ}$  and slightly north of the Galactic plane. Because of its morphology this area has been referred to as the "fan region". The polarized emission is believed to be of local origin. The derived Rotation measures are small (e.g. Bingham & Shakeshaft 1967) and the magnetic field direction has to be basically orientated perpendicular to

the line of sight. However, in addition to the large-scale component, which we add from the Dwingeloo survey, a lot of small-scale variations are visible (Fig. 10).

# 4.4. The anticentre region

Fig. 12 to Fig. 14 display the results of the anticentre region north of the Galactic plane. Color images (Fig. 13) of the total intensity and polarization intensity in the direction of the Galactic anticentre show the polarization features and absence of corresponding total-power emission in detail. Although an absolute calibration of the polarized emission on large scales was not possible because of missing Dwingeloo data, significant small-scale polarization is found across the area. The most remarkable structures are apparently depolarized features (Fig. 13), which form filaments (e.g. at  $\ell = 204^{\circ}$ ,  $b = 12^{\circ}$  or  $\ell = 206^{\circ}$ ,  $b = 9^{\circ}$ ) or ring-like structures (e.g. at  $\ell = 191^{\circ}$ ,  $b = 9^{\circ}$  or at  $\ell = 196^{\circ}5, \ b = 5^{\circ}5)$  with sizes up to about 3°. The depolarized features have no counterpart in the small-scale total intensity emission (Fig. 12, 13) or the large-scale component (Fig. 14). Depolarization can be caused either by some filamentary thermal matter with enhanced electron density, by magnetic field variations in strength and/or direction or the superposition of magnetic field components in the line of sight with orientations perpendicular to each other. Higher frequency observations with the 100-m telescope are underway to clarify the nature of these features.

# 5. Concluding remarks

The maps shown include information on a wealth of faint emission structures at medium Galactic latitudes. The total intensities decrease quickly with increasing distance from the plane as is expected for a thin disk of emission. Strong sources become rare, but faint extended ridges, arcs and more or less structured discrete emission regions are seen superimposed on the still dominating unresolved Galactic emission.

There is substantial diffuse polarized emission seen in all the observed fields. This emission is characterized by fluctuations on angular scales of the beam size up to several degrees. Interestingly, there exist significantly polarized regions of the order of several degrees in size, which have no corresponding structures in the total-power emission. Moreover, within the polarized emission there are numerous nearly straight, loop or arc shaped structures, which seem to be depolarized. They are most pronounced in the direction of the Galactic anticentre, where the line of sight across the Galaxy is comparably short. In these regions, the total intensity of diffuse Galactic emission as revealed from the Stockert 1.4 GHz survey is less than 0.5 K. In view of the observed polarized intensities of up to 0.25 K, there are also areas with well organized magnetic fields and quite small Faraday rotation effects. The most likely explanation for the small-scale structures are significant spatial variations of the Faraday rotation by the interstellar medium in the line of sight, which modulate a significantly polarized smooth Galactic diffuse emission. It is not clear whether fluctuations of the Galactic magnetic field or changes in the electron density are the reason for that. We conclude that probing the properties of the diffuse Galactic emission via a polarization survey is a promising tool towards the improvement of our current understanding of the Galaxy and the local ISM.

#### References

Beck R., Brandenburg A., Moss D., Shukorov A., Sokoloff D., 1996, ARA&A 34, 155

Bingham R.G., Shakeshaft J.R., 1967, MNRAS 136, 347 Brouw W.N., Spoelstra T.A.Th., 1976, A&AS 26, 129

Cash W., Garmire G., Riegler G., 1980, ApJ 133, 67

Condon J.J., Broderick J.J. Seielstad G.A., 1989, AJ 97, 1604
Condon J.J., Cotton W.D., Greisen E.W., Yin Q.F., Perley R.A., Taylor G.B., Broderick J.J., 1998, AJ 115, 1693

Duncan A.R., Haynes R.F., Jones K.L., Stewart R.T., 1997, MNRAS 291, 279

Duncan A.R., Reich P., Reich W., Fürst W., 1999, A&AS (in press)

Fürst E., Reich W., Reich P., Reif K., 1990 A&AS 85, 691
 Gray A.D., Landecker T.L., Dewdney P.E., Taylor A.R., 1998,
 Nat 393, 690

Junkes N., Fürst E., Reich W., 1987a, A&AS 69, 451

Junkes N., Fürst E., Reich W., 1987b. In: Beck R., Gräve R. (eds) Interstellar Magnetic Fields. Springer, Heidelberg, p. 146

Reich P., Reich W., 1986, A&AS 63, 205

Reich P., Reich W., Fürst E., 1997, A&AS 126, 413

Reich W., 1982, A&AS 49, 219

Reich W., Reich P., Fürst E., 1990a, A&AS 83, 539

Reich W., Fürst E., Reich P., Reif, K., 1990b, A&AS 85, 633 Salter C.J., Brown R.L., 1988. In: Verschuur G.L., Kellermann

K.I. (eds.) Galactic and Extragalactic Radio Astronomy. Springer, p. 1

Sofue Y., Reich W., 1979, A&AS 38, 251

Uyanıker B., 1997, PhD Thesis, Bonn University

Uyanıker B., Fürst E., Reich W., Reich P., Wielebinski, R., 1998, A&AS 132, 401 (Paper I)

Wielebinski R., 1992. In: Krause F. et al. (eds.) Proc. IAU Symp. 157, The Cosmic Dynamo. Kluwer, Dordrecht, p. 271

Wieringa M.H., de Bruyn A.G., Jansen D., Brouw W.N., Katgert P., 1993, A&A 268, 215

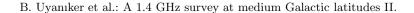


Fig. 2. Small-scale total intensity image of the region towards  $\ell=50^\circ$  with superimposed polarization vectors in the E-field direction. Galactic coordinates are shown. The first contour set starts from 0 mK  $T_B$  and runs in steps of 120 mK  $T_B$  and the second contour set starts at 600 mK  $T_B$  and runs in steps of 240 mK  $T_B$ . The wedge at the top shows the lower and upper cuts of the image. Every second polarization vector is plotted and a vector of 2' length corresponds to 100 mK  $T_B$  in polarized intensity.

6	B. Uyanıker et al.: A 1.4 GHz survey at medium Galactic latitudes II.
Fig. 3. Filtered large-sca	ale total intensities of the area shown in Fig. 2. Contours start at 4500 mK $T_{\rm B}$ and run in
steps of 50 mK $T_B$ . The	beam width of the filter was 3°.





sets start at 0 mK T<sub>B</sub>, 800 mK T<sub>B</sub> and 1800 mK T<sub>B</sub> (white contours) and run in steps of 150 mK T<sub>B</sub>, 300 mK T<sub>B</sub> and 750 mK T<sub>B</sub>, respectively. The right panel shows the total intensity map towards the southern part of the Cygnus region. The contours start at 0 mK T<sub>B</sub> and run in steps of 150 mK T<sub>B</sub>. The contours plotted in white start at  $1200 \text{ mK T}_{\text{B}}$  and run in steps of  $400 \text{ mK T}_{\text{B}}$ . In both of the panels the electric field vectors are scaled to the polarized intensity and 100 mK T<sub>B</sub> represented with a bar of length 8'. Every third vector is plotted.



Fig. 6. Large-scale total intensity map towards the northern part of the Cygnus region is shown in the left panel. The first contour set starts at 4160 mK  $T_B$  and run in steps of 50 mK  $T_B$  and the second contour set starts at 4800 mK  $T_B$  and run in steps of 300 mK  $T_B$ . Cyg A at about  $\ell \sim 76^\circ$  is blanked. The right panel displays the large-scale total intensity map towards the southern part of the Cygnus region. The contour set starts at 4300 mK  $T_B$  and run in steps of 50 mK  $T_B$ 





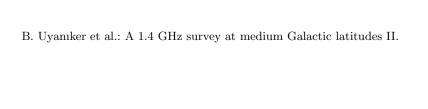
Fig. 8. Total intensity map close to  $\ell \sim 140^\circ$ . Contours start at 0 mK  $T_B$  and run in steps of 100 mK  $T_B$ . Small-scale polarization data are overlaid as vectors such that 100 mK  $T_B$  corresponding to a bar of length 6'. Every second vector is plotted.





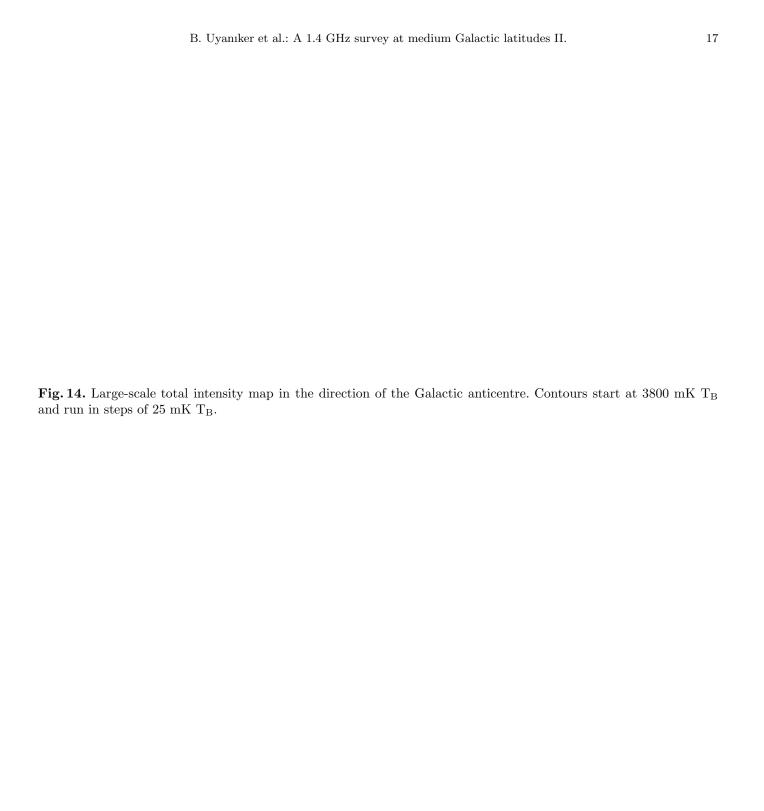
Fig. 10. Polarized intensity map of the small-scale emission near  $\ell \sim 140^\circ$ . Contours start at 0 mK  $T_B$  and run in steps of 50 mK  $T_B$ . This map partly covers the field from which the highest polarization emission in the Galaxy is observed.

14	B. Uyanıker et al.: A 1.4 GHz survey at medium Galactic latitudes II.
Fig. 11. Large-scale polar	rized intensity map near $\ell \sim 140^\circ$ . Contours start at 380 mK $T_B$ and run in steps of 15 mK $T_B$ .
1 18. 11. Earge seare point	The differentially map from v 110. Contours source at 500 mil 15 and 1 and m 500pt of 10 mil 15.



15

Fig. 12. Total intensity intensity map of the small-scale emission in the direction of the Galactic anticentre. Contours start at 0 mK  $T_B$  and run in steps of 50 mK  $T_B$ . Overlaid bars are electric field vectors such that 100 mK  $T_B$  corresponds to 4'. Every second vector is plotted.



This figure "fig1.gif" is available in "gif" format from:

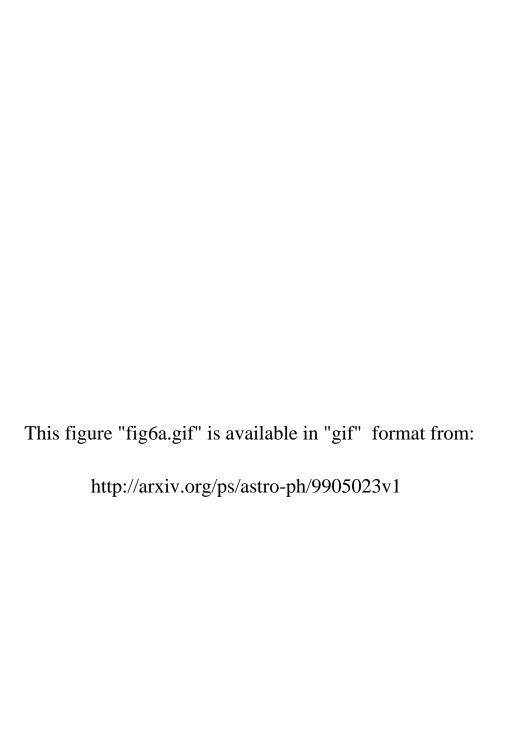
This figure "fig2.gif" is available in "gif" format from:

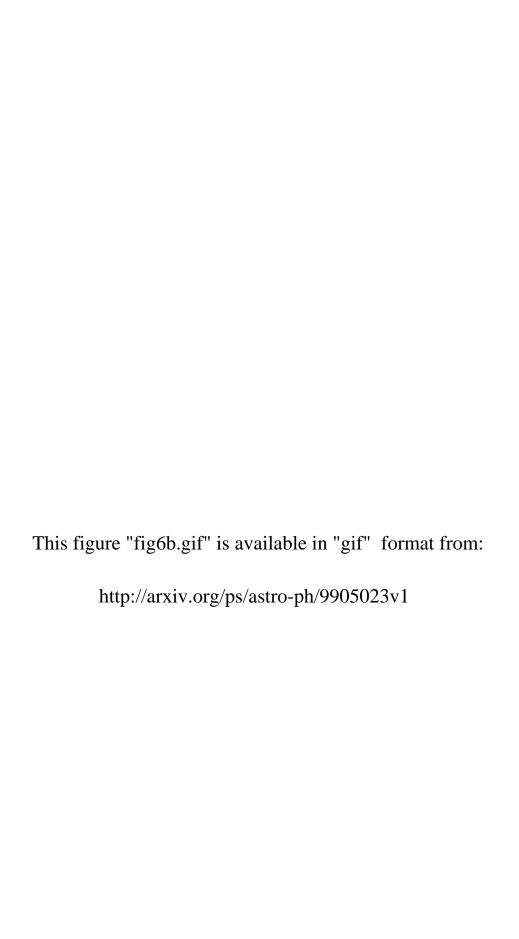
This figure "fig3.gif" is available in "gif" format from:

This figure "fig4.gif" is available in "gif" format from:

This figure "fig5a.gif" is available in "gif" format from:

This figure "fig5b.gif" is available in "gif" format from:





This figure "fig7a.gif" is available in "gif" format from:

This figure "fig7b.gif" is available in "gif" format from:

This figure "fig8.gif" is available in "gif" format from:

This figure "fig9.gif" is available in "gif" format from:

This figure "fig10.gif" is available in "gif" format from:

This figure "fig11.gif" is available in "gif" format from:

This figure "fig12.gif" is available in "gif" format from:

This figure "fig13a.gif" is available in "gif" format from:

This figure "fig13b.gif" is available in "gif" format from: http://arxiv.org/ps/astro-ph/9905023v1

This figure "fig14.gif" is available in "gif" format from: